SLAC-PUB-2989
October 1982
(T/E)

REVIEW OF e^+e^- PHYSICS AT PEP - 1982*

Robert Hollebeek
Stanford Linear Accelerator Center
Stanford University, Stanford, California 94305

ABSTRACT

Results obtained at PEP by the MARK II, MAC and DELCO collaborations in the past year are reviewed. They include QED tests, measurements of τ lepton properties, charm and bottom fragmentation functions, scaling violations, energy correlations and the total hadronic cross section.

I. INTRODUCTION

After a brief discussion of the PEP machine and its experiments (Sections II and III), the physics of high energy electron and positron collisions will be discussed. This interaction provides many opportunities for testing our ideas about fundamental physics. This is at least partially due to the fundamental nature of the electron or positron itself which as far as we know now has no internal structure. It is also due however to the simple nature of the interactions of these particles. We have no evidence that they participate directly in strong interactions and hence we can apply the very successful theory of QED to their interactions. The simplest final states where the electron and positron have annihilated to produce pairs of muons, electrons, or tau's, allow us to test the detailed predictions of QED and look for the effects of the weak interactions of these leptons. Section IV discusses these tests of QED and leptonic weak interactions.

Energy and momentum conservation require that a pair of particles be produced back-to-back in the center-of-mass. States which have two leptons which do not balance momentum in this way can arise from two sources. The first source is a correction to the simplest prediction of QED and results in a final state with two leptons and some photons or four leptons. These interactions are in general suppressed by factors of order α the fine structure constant ($\sim 1/137$). This suppression allows us to test for the second source - new particles which are produced in pairs but subsequently decay into leptons. The heavy lepton τ was discovered this way, and its properties are discussed in Section V. Other searches for excited leptons, scalar leptons, Higgs particles and other heavy leptons have all been negative.

In the earliest days of the study of e^+e^- interactions, the most surprising feature was the copious production of strongly interacting particles. We now understand the mechanism in analogy to the QED production of pairs of leptons. We believe that these states arise from the production of pairs of charged quarks which then fragment into observed particles. The final state which results is not a pair of back-to-back particles as in the case of QED, but a pair of back-to-back jets. The remaining Sections VI-XI discuss these hadronic final states and what we can learn about quarks from them. We now have a candidate theory QCD or quantum chromodynamics which appears to describe many of the features of these states. Unfortunately, there are reasons why detailed predictions in this theory are much more difficult to obtain than in QED. Nevertheless, we have begun to study the higher order processes in QCD by looking at final states where the jets are not back-to-back or where there appear to be more than two jets.

Finally in Section XII we summarize the results which have been obtained so far and indicate the areas where future work will concentrate.

II. THE PEP MACHINE

PEP is an electron and positron storage ring constructed jointly by the Stanford Linear Accelerator Center and the Lawrence Berkeley Laboratory. Construction began in June 1977 and was completed in April of 1980. First beam was stored on April 16 and machine studies began. Efforts since that time have concentrated on operating the storage ring at 14.5 GeV, an energy where the SLAC linac could inject both positrons and electrons directly into the ring.

The ring itself is designed to operate in the 5 to 18 GeV energy range for a single beam. The layout on the SLAC site is indicated schematically in Fig. 1. Electrons are injected directly into the ring as are

* Work supported by the Department of Energy, contract DE-AC03-76SF00515.

(Invited talk presented at the VI European Symposium on Nucleon Antinucleon and Quark Antiquark Interactions, Santiago de Compostella, Spain, August 30 - September 3, 1982.)

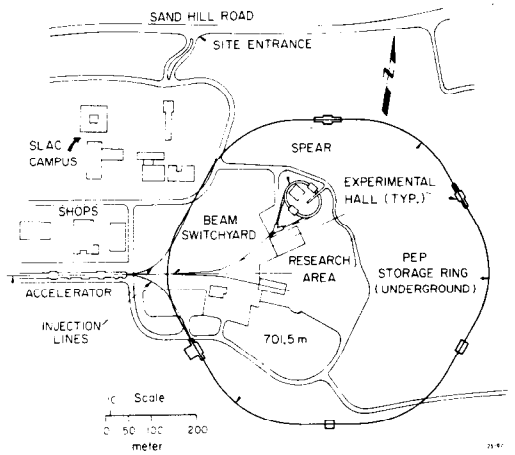

Fig. 1. Layout of the PEP ring on the SLAC site.

positrons produced in a target 1/3 of the way down the linear accelerator. This means that the storage ring can operate over most of its energy range without having to ramp the energy of the stored beams from injection energy to final energy. The ring has a circumference of 2.2 km, six interaction regions for experimentation and runs with three counter rotating bunches in each beam. Between each interaction region is a symmetry section where the beams do not collide, hence the six interaction regions are called regions 2, 4, 6, 8, 10, and 12.

The period between April 1980 and January 1981 was devoted to machine physics although some luminosity was recorded by the experimenters. During the period of January to June 1981 the ring began serious operation for physics and produced 16,000 nb^{-1} of integrated luminosity all at 29 GeV in the center-of-mass system.

The luminosity $\mathscr{L}$ is the parameter of the machine which determines how many events an experimenter will see since the event rate R and the cross-section for any process are related by

$$R = \mathscr{L}\sigma \ .$$

For example, the muon pair cross sections at 29 GeV is 10^{-1} nb and an integrated luminosity of 16,000 nb^{-1} will result in of order 1600 events times the detection efficiency of the experiment.

During the summer of 1981, the Q1 quadrupoles (the closest to the interaction region) were moved from their old positions at 11 meters from the interaction point to 7.4 meters in order to reduce the betatron function of the machine there. The beam size is proportional to the square root of the betatron function and the luminosity is inversely proportional to the beam area. Hence reducing the betatron function should increase the luminosity. The initial movement of the Q1's however produced a large value of the betatron function in the region of the RF cavities and this had to be corrected by moving the cavities in the Christmas shutdown.

Physics running began again in February 1982 and the machine produced an additional 30,000 nb^{-1} during that time. Average luminosity during this period was 230 nb^{-1} per day and peak luminosities of over 10^{31} cm^{-2} sec^{-1} were achieved. Experience with the PETRA and CESR storage rings indicates that the performance of the machine can be further improved by also moving the second quadrupole Q2 closer to the interaction region. This work was completed during the summer 1982 shutdown together with the installation of additional klystron power supplies, and vertical correction magnets near the interaction regions.

III. THE EXPERIMENTS

The six interaction regions at PEP are occupied at present by the experiments shown in Table 1. The TPC (time projection chamber) detector was installed in IR-2 in January 1982 and used the spring cycle mainly for checkout of the experiment. The TPC detector and the PEP-9 two gamma experiment have implemented a two-way data link so that information from the central detector can be available on events where electrons are observed in the forward detector. The TPC and two gamma detectors are shown together in Fig. 2. Interaction region 4 contains the MAC detector shown in Fig. 3. The MAC detector covers the region $|\cos\theta| < 0.95$ with electromagnetic and hadronic calorimetry. This large acceptance is important in increasing the efficiency of the device for event detection, and is being used in the measurement of the total

Table 1. Current PEP Experiments

Interaction Region	Experiment	Purpose
2	PEP-4, PEP-9	TPC and Two Photon Facility
4	PEP-6	MAC-Calorimetric Detector
6	PEP-12	HRS - High Resolution Spectrometer
8	PEP-20	DELCO - Cerenkov Detector
10	PEP-2	Search for Highly Ionizing Particles
12	PEP-5	MARK II - General Purpose Detector

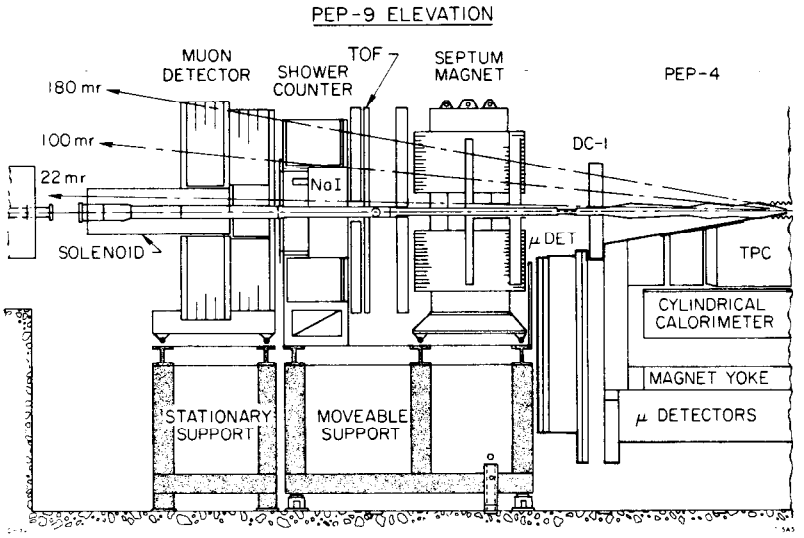

Fig. 2. TPC (PEP-4) and two gamma (PEP-9) detectors.

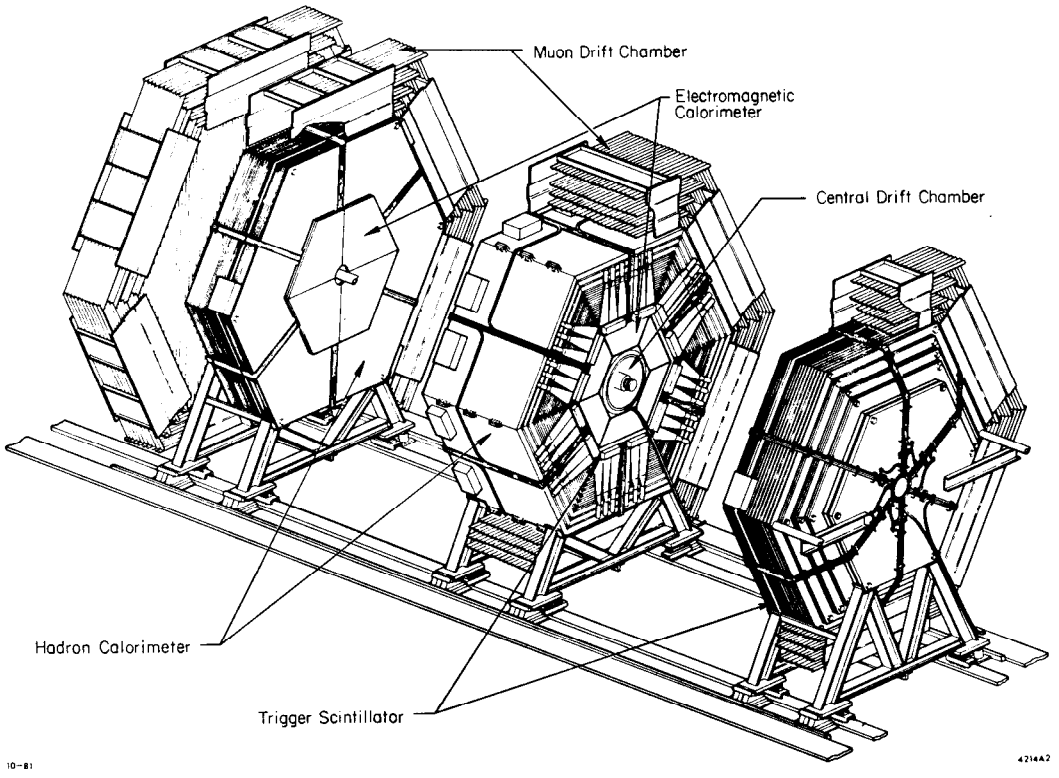

Fig. 3. MAC detector.

cross-section to study the effect of model dependent corrections to the cross-section for finite apparatus solid angle. The experiment collected an additional 26,000 nb^{-1} of data in the spring cycle to be added to a previous sample of 7,000 nb^{-1}.

The next interaction region contains the HRS or high resolution spectrometer (Fig. 4). This device is based on the 2 meter diameter superconducting magnet of the Argonne 12 foot bubble chamber which provides a large volume magnetic field of 1.6 Telsa. Inside the magnet is an inner drift chamber of radius 1.1 meters which has achieved a resolution of 170 microns. During the summer months a system of ultraviolet photoionizing Cerenkov counters is being installed. These together with the electromagnetic calorimeters are inside the magnetic field volume. With the completion of the high pressure Cerenkov system, this experiment will have unique capabilities in high momentum particle separation.

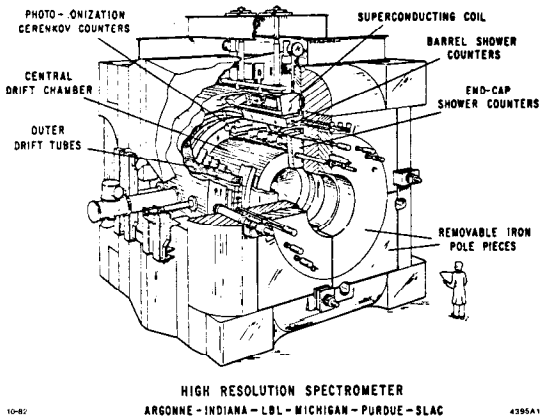

Fig. 4. HRS detector.

Region 8 contains the DELCO detector (Fig. 5) which collected 23,000 nb^{-1} of data. Their event sample contains about 8,000 hadronic events. The chief feature of this experiment is the Cerenkov device which is used to tag low energy electrons as well as high momentum kaons and protons. The mean number of photoelectrons in the Cerenkov is 18 which is important for reliable identification of particles above threshold. During the summer of 1982 a new vacuum chamber with a wide bore and thin center section will be installed to reduce beam backgrounds to the low energy electron sample. This sample is important for the study of heavy charmed or bottom meson production via their semi-leptonic decays.

Region 10 contains an array of LEXAN and CR-39 plastic detectors which are being used to search for monopoles or other highly ionizing particles. Initial

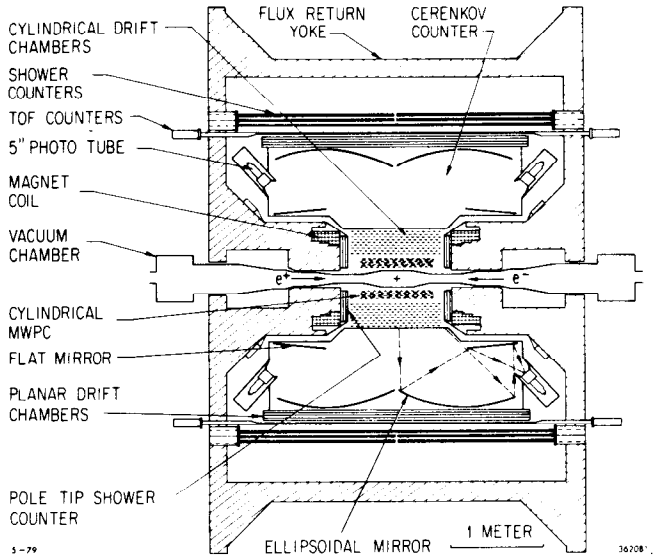

Fig. 5. DELCO detector.

results from this experiment[1] placed a 90% confidence level limit on their production at 2.5×10^{-3} nb based on 8.4×10^{3} nb^{-1} of data. During the spring cycle, an additional 30.8×10^{3} nb^{-1} of data were collected and these are currently being scanned for events.

Finally, region 12 contains the MARK II detector (Fig. 6) which was constructed and debugged at SPEAR and moved to PEP as soon as the machine was finished. The detector collected 15,000 nb^{-1} of data before the spring cycle. Due to a short in the magnet coil, however, six weeks of data were lost in the spring cycle. The magnet has been repaired and is now

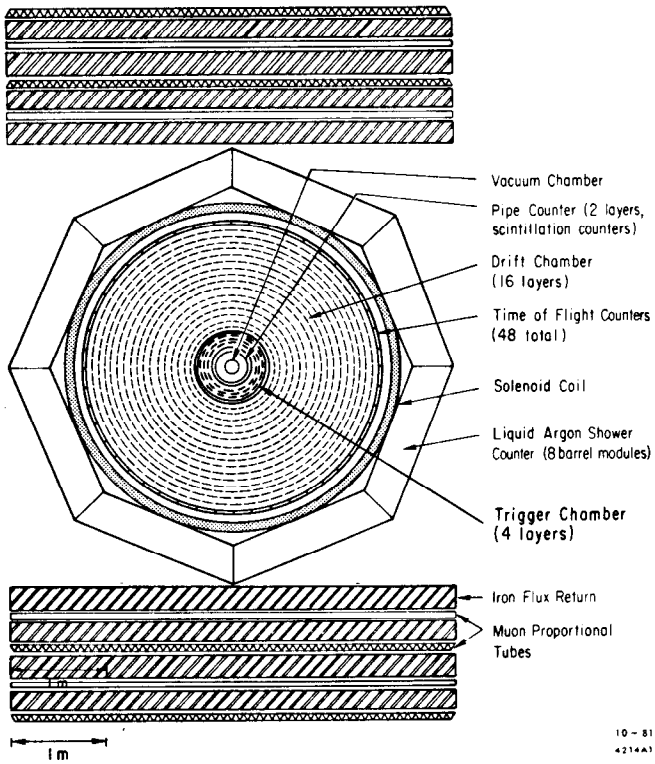

Fig. 6. MARK II detector.

running at half field. The momentum resolution of the MARK II is approximately the same as in previous data at full field due to the use of a new vertex detector in the track fits. The total data sample consists of 38×10^3 nb^{-1} which corresponds to ~15,000 hadronic events. The collaboration is concentrating on the analysis of hadronic final states and the use of the vertex detector capabilities for lifetime measurements and heavy meson tagging.

IV. QUANTUM ELECTRODYNAMICS

The simplest final states which are observed at electron-positron storage rings are the annihilation of the initial particles into a pair of leptons or a pair of photons. Each of these cross-sections can be calculated using quantum electrodynamics. This theory embodies Maxwell's equations in a quantum framework. Low energy tests have found that the theory is very successful in predicting the features of atomic spectra, fine splittings, properties of mu-mesonic atoms, and magnetic moments of electrons and muons. These tests however do not probe another significant assumption in the theory which is that leptons have no internal structure. This is best done at high energy where the basic 1/s behavior of point corss-sections would be modified by the appearance of form factors. No test so far has given any indication that the theory is incorrect and in fact, to test for the effect of including weak interaction effects which are comparable to higher order QED processes at currently available energies, we must assume that it is correct.

The reactions which are available for these tests are

$$e^+e^- \rightarrow \gamma\gamma$$
$$e^+e^- \rightarrow e^+e^-$$
$$e^+e^- \rightarrow \mu^+\mu^-$$
$$e^+e^- \rightarrow \tau^+\tau^- \quad .$$

The lowest order diagrams for the process $e^+e^- \rightarrow \gamma\gamma$ are shown in Fig. 7. This process is unique among the two body QED final states in that it is not modified to lowest order by contributions from the weak interactions.[2] The modifications to lowest order QED involve either the inclusion of a new heavy electron which couples to $e\gamma$ or a modification of the electron propagator and vertex function. They are parameterized by two forms;

$$\frac{d\sigma}{d\Omega} = \frac{d\sigma_{QED}}{d\Omega}\left(1 \pm \frac{s^2 \sin^2\theta}{2\Lambda_\pm^4}\right)$$

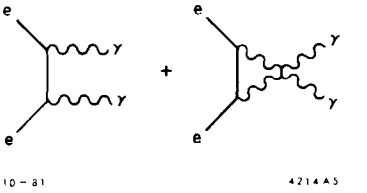

Fig. 7. QED diagrams for $e^+e^- \rightarrow \gamma\gamma$.

and

$$\frac{d\sigma}{d\Omega} = \frac{d\sigma_{QED}}{d\Omega}\left(1 \pm \frac{s^2 \sin^2\theta}{2\Lambda_\pm^4(1+\cos^2\theta)}\right)$$

where $d\sigma_{QED}/d\Omega = (\alpha^2/s)(1+\cos^2\theta/\sin^2\theta)$. In the first case, Λ_+ can be interpreted as a limit on the contribution of a heavy electron with mass m_{E^*} and charge e^* in which case $\Lambda_+ = m_{E^*}\sqrt{e/e^*}$. The parameter Λ_- has no similar interpretation. The second form results from an attempt to modify the electron propagator. The Ward identity, a consequence of gauge invariance and charge conservation, requires in QED that a modification to the electron propagator be accompanied by a modification to the vertex function. The general constraints for such modifications have been analyzed by Kroll.[3] A physical model for such a modification would require substructure for the electron (non-pointlike vertex function) produced for example by a neutral object which couples to the electron.

The experimental angular distribution of γ pair events from the MARK II detector with 14.4 pb^{-1} is shown in Fig. 8. The curve is the expected distribution from QED to order α^3 as calculated by the Berends-Kleiss Monte Carlo.[4] Figure 9 shows the data from the MAC detector normalized to the QED cross-section. The integrated luminosity is 14 pb^{-1}. The Λ parameters determined from these data together with similar results from PETRA experiments[5] are shown in Table 2.

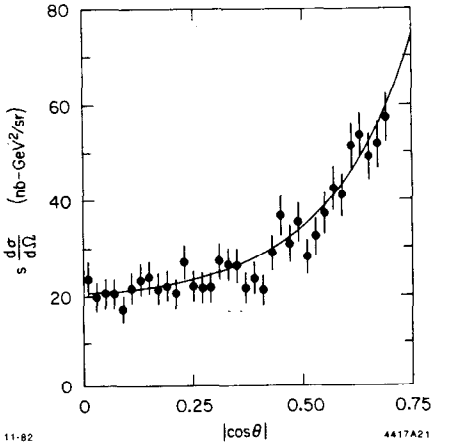

Fig. 8. MARK II $e^+e^- \rightarrow \gamma\gamma$ data with QED to order α^3.

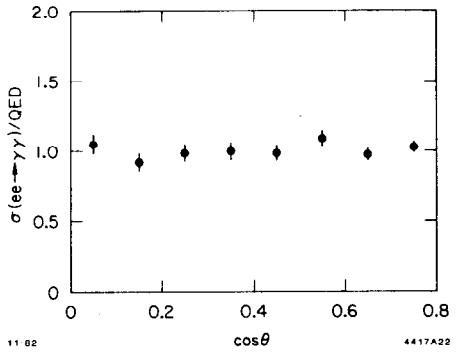

Fig. 9. MAC $e^+e^- \to \gamma\gamma$ normalized to σ_{QED}.

Table 2. QED Λ Parameters for $e^+e^- \to \gamma\gamma$

	Excited Electron		Modified Propagator	
	Λ_+	Λ_-	Λ_+	Λ_-
MAC	55	53	50	51
MARK II	49	39	46	40
CELLO	43	48		
JADE	47	44		
MARK-J	51	49	51	41
PLUTO	46		46	36
TASSO	34	42		

These results indicate that we can eliminate heavy leptons and neutral objects with standard coupling strength e up to a mass of ~50 GeV.

The analysis of QED tests in the case of electron, muon and tau pair final states is complicated by the modifications due to neutral weak currents. In addition to the normal QED diagrams, diagrams must be included where the photon has been replaced by the neutral weak boson Z^o as shown in Fig. 10. The weak contributions to the μ pair and e pair cross sections have been calculated by R. Budny[6] including the effects of polarization. For the μ pairs, the cross section is of the form

$$\frac{d\sigma}{d\cos\theta} = \frac{\pi\alpha^2}{2s}\left[(1+B)\cos^2\theta + A\cos\theta\right]$$

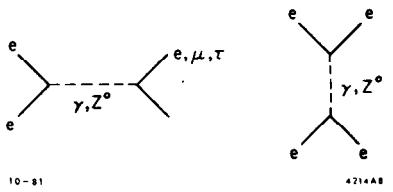

Fig. 10. Weak and electromagnetic diagrams for lepton pair production.

where

$$B = -8 g_V^2 gs\left(\frac{m_Z^2}{m_Z^2-s}\right) + 16\left(g_A^2+g_V^2\right)g^2 s^2\left(\frac{m_Z^2}{m_Z^2-s}\right)^2$$

$$A = -16 g_A^2 gs\left(\frac{m_Z^2}{m_Z^2-s}\right) + 128 g_A^2 g_V^2 g^2 s^2\left(\frac{m_Z^2}{m_Z^2-s}\right)^2$$

$$g = 4.49\times10^{-5}\ \text{GeV}^{-2} \quad .$$

The B term modifies the total cross section while the A term results in a forward-backward asymmetry. Note however that the B term is quite small because the measured value of $\sin^2\theta_W$ is close to 0.25 at which value $g_V = 0$. Current measurements[7] of g_A are consistent with the value of 0.5 expected from the standard weak isospin assignments of Weinberg and Salam. With these values, the weak effects change the total cross section by ~0.1% an amount which is small compared to systematic errors, but give an asymmetry of order 6-7% at PEP. The asymmetry is negative below the Z pole. The weak corrections affect the e^+e^- and $\mu^+\mu^-$ final states differently. Values of g_V consistent with neutrino interactions can change the total cross section and form of the angular distribution for electron pairs at the several percent level. Increasing g_V^2 increases the Bhabha cross section while decreasing the muon cross section slightly. Thus the greatest sensitivity to g_V comes from the ratio of the normalizations of the Bhabha and muon pair cross sections while the value of g_A^2 is determined primarily from the muon asymmetry.

To be sensitive to effects in the cross sections at the few percent level, it is important to treat the higher order corrections of QED itself. Radiative effects for example in the μ pair case cause a forward backward asymmetry due to the interference of the one photon (c = -1) and two photon (c = +1) intermediate states. The size of this asymmetry depends on the momentum and acoplanarity cuts used in the analysis. Both the MAC and the MARK II groups use the Berends-Kleiss Monte Carlo to calculate the expected experimental distributions to order α^3.

The data on the Bhabha cross section from the MAC group is shown in Fig. 11 based on a sample of 25 pb^{-1} at $\sqrt{s}$ = 29 GeV. The analysis of the MARK II group is based on a sample of 14 pb^{-1} and is shown in Fig. 12. The MAC group fits for the single parameter $\sin^2\theta_W$ and finds

$$\sin^2\theta_W = 0.24 \pm 0.10$$

and at the 95% confidence level

$$0.05 \le \sin^2\theta_W \le 0.44 \quad .$$

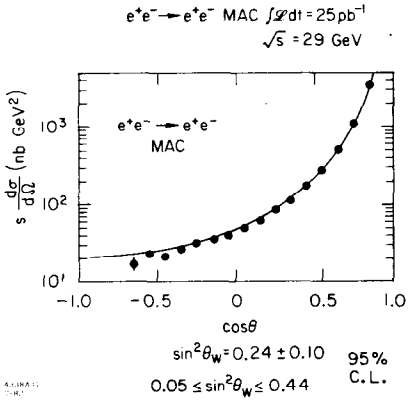

Fig. 11. MAC $e^+e^- \to e^+e^-$ with α^3 QED prediction.

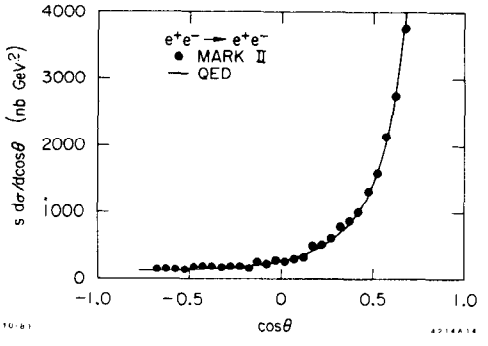

Fig. 12. MARK II $e^+e^- \to e^+e^-$ with α^3 QED prediction.

The MARK II group has made a joint fit to the e and μ pairs to simultaneously determine g_A^2 and g_V^2 and finds

$$g_A^2 = 0.24 \pm 0.16$$

$$g_V^2 = 0.05 \pm 0.10 \quad .$$

The data for the muon pair angular distributions from the MARK II and MAC groups are shown in Figs. 13 and 14. The observed asymmetries within the solid angle, the expected value from Weinberg-Salam and the fits for $g_A^e\ g_A^\mu$ are shown in Table 3. A new measurement of the muon pair asymmetry at low energies where

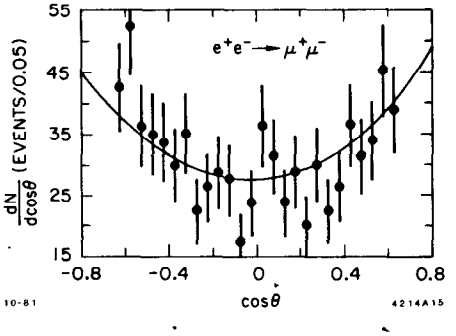

Fig. 13. MARK II $e^+e^- \to \mu^+\mu^-$ with α^3 QED prediction.

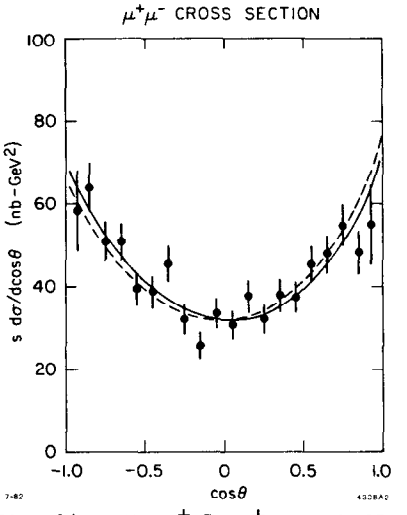

Fig. 14. MAC $e^+e^- \to \mu^+\mu^-$ with QED and QED + WEAK predictions.

Table 3. MARK II and MAC fits to $e^+e^- \to \mu^+\mu^-$

	A_μ (observed)	A_μ (Weinberg-Salam)	$g_A^e\ g_A^\mu$
MARK II	-5.2±3.2 %	- 4.5 %	0.32±0.18±0.02
MAC	-4.4±2.4 %	- 6.3 %	0.18±0.10

the weak effects are expected to be small has been made with the data taken by the MARK II collaboration at SPEAR. The data is shwon in Fig. 15. The results of fits to the angular distribution are shown in Table 4 together with earlier results from the MARK I collaboration.[8] A compilation of measurements showing the variation of the asymmetry with center-of-mass energy is shown in Fig. 16 together with the expected behavior in the Weinberg-Salam model ($g_A^2 = 0.25$) for a Z^o mass of $m_Z = \infty$ and $m_Z = 90$ GeV. Systematic errors of order 1% are still comparable to the expected difference between Weinberg-Salam ($m_Z \sim 90$ GeV) and pure weak interactions ($m_Z \to \infty$).

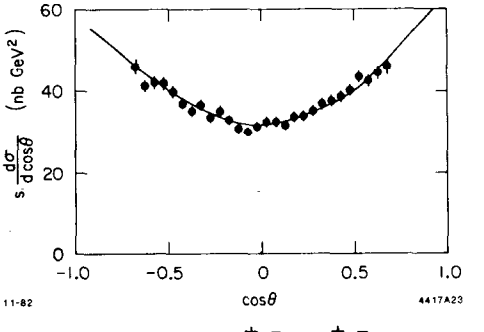

Fig. 15. MARK II $e^+e^- \to \mu^+\mu^-$ at $\langle E_{c.m.} \rangle^{\frac{1}{2}} = 5.847$ compared to $1 + \cos^2\theta$.

Table 4. MARK II and MARK I $e^+e^- \to \mu^+\mu^-$ at low energy

	$\langle E^2_{c.m.} \rangle^{\frac{1}{2}}$	A_μ (observed)	$g^e_A\, g^\mu_A$
MARK II	5.847	1.2 ± 0.7 %	-1.6 ± 0.9
MARK I	6.8	-0.3 ± 1.0 %	

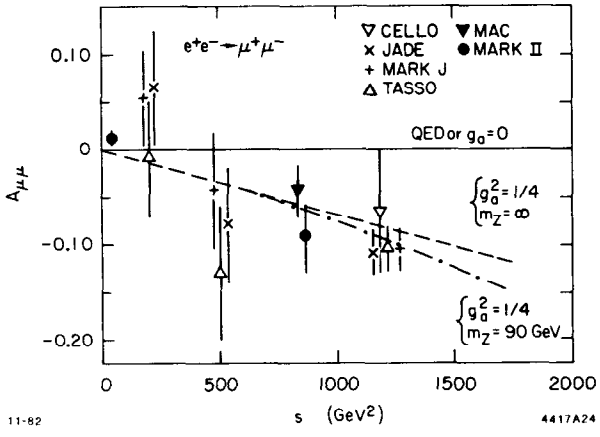

Fig. 16. $A_{\mu\mu}$ vs s from SPEAR, PEP and PETRA.

The tau pair cross section has been measured by the MAC and MARK II groups using μe final states. The data and QED predictions are shown in Figs. 17 and 18. The asymmetry measured by the MAC collaboration for this reaction is

$$A_{\tau\tau} = -0.013 \pm 0.029 \quad (-0.063 \text{ expected})$$

which yields

$$g^e_A\, g^\tau_A = 0.05 \pm 0.11 \quad .$$

The MARK II fit gives

$$A_{\tau\tau} = -0.032 \pm 0.050 \quad (-5.0 \text{ expected})$$

and

$$g^e_V\, g^\tau_V = 0.16 \pm 0.26$$

$$g^e_A\, g^\tau_A = 0.19 \pm 0.29 \quad .$$

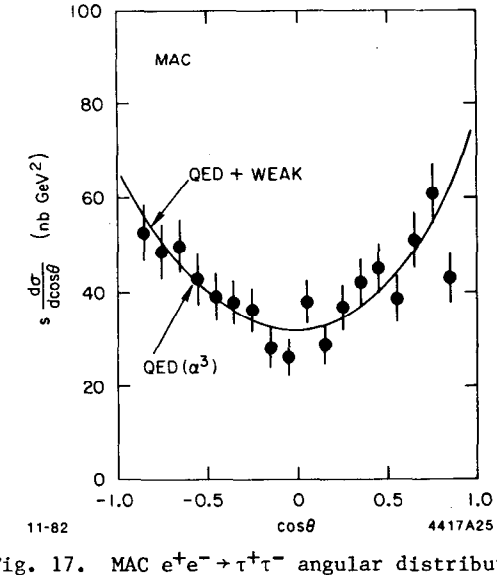

Fig. 17. MAC $e^+e^- \to \tau^+\tau^-$ angular distribution.

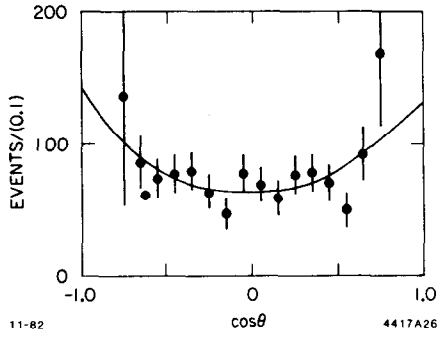

Fig. 18. MARK II $e^+e^- \to \tau^+\tau^-$ angular distribution.

The normalization of the MARK II data has been used to place a limit on possible compositeness of the τ lepton. The measured value

$$\frac{\sigma_{\tau\tau}}{\sigma_{QED}} = 0.97 \pm 0.05 \pm 0.05$$

yields cutoff parameters for the τ of

$$\Lambda_+ = 134 \text{ GeV}$$
$$\Lambda_- = 103 \text{ GeV}$$

equivalent to testing the structure of the τ to a distance of order 2×10^{-16} cm. The measurements from the MARK II and PETRA are shown in Fig. 19.

In conclusion, all tests indicate that the production of photon pairs and lepton pairs is well described by the combination of QED and the simplest version of the unified weak and electromagnetic theories ($g_A^2 = \frac{1}{4}$, $g_V^2 = 0$). Tests indicate that the heavier τ lepton is as pointlike as the muon and that e, μ, τ universality describes the couplings of these leptons.

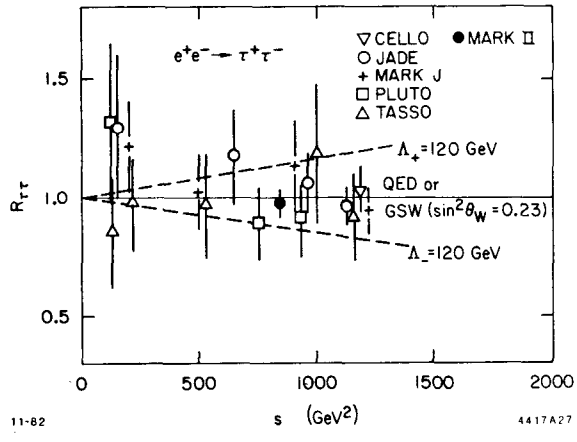

Fig. 19. Ratio of the $e^+e^- \to \tau^+\tau^-$ cross section to the point cross section.

V. PROPERTIES OF THE τ LEPTON

The energy range of the PEP machine is well suited to the study of the final states which result from the weak decays of this heavy lepton. At lower energies, the identification of $\tau^+\tau^-$ events is difficult because the multiplicities and sphericities or angular distributions of the decay products are similar to hadronic final states. If the energy of the produced pairs is too high, the final state products are highly collimated and difficult to unfold. One of the most interesting questions which remain about the τ lepton is that the sum of both the measured and calculated decay modes is only 76%.[9] One prong modes which have been measured include $e\nu\nu$, $\mu\nu\nu$, $\pi\nu$, $\rho\nu$, $K^*\nu$, $\pi^\pm 2\pi^o\nu$, $\pi^\pm 3\pi^o\nu$, and $\pi^\pm 4\pi^o\nu$. Three prong modes seen are $3\pi^\pm\nu$, $3\pi^\pm\pi^o\nu$, and $3\pi^\pm 2\pi^o$. The MAC and MARK II detectors have both placed limits on the possible contribution of 5 prong modes and measured the one and three prong branching ratios. The results are shown in Table 5.

Table 5. Branching Ratios for the τ

	MAC	MARK II
N_τ	470	705
Background	64 ± 7	98
B_1	0.86 ± 0.04 ± 0.01	0.86 ± 0.015 ± 0.01
B_3	0.153 ± 0.007 ± 0.01	0.14 ± 0.02
B_5	< 0.007	< 0.005

Given the small limits placed on possible five prong modes, the missing modes must be one prong modes possibly 1 charged + $5\pi^o$, etc. An alternative explanation is that since all the measurements are normalized to the leptonic decay modes that there is a small fractional error in this measurement. The three prong modes measured at PEP are higher than previous measurements at lower energy machines such as SPEAR and DORIS (0.68 ± 0.10) but are in good agreement with the results of the TASSO and CELLO detectors at PETRA (0.76 ± 0.06 and 0.84 ± 0.02).

The DELCO detector has used their Cerenkov detector to measure the ratio of π and K mesons in the $\tau \to 1$ prong data sample. For particles with momenta greater than 4 GeV, the mean number of photoelectrons from pions is approximately 25. Kaon candidates are those prongs with fewer than three photoelectrons. The resulting sample of 13 events with an estimated background of two events determines the Cabbibo angle in τ decay yielding

$$\tan^2\theta_c = 0.08 \pm 0.03 \pm 0.04 \quad .$$

Finally, since the first measurement of the lifetime of the τ lepton by the MARK II collaboration[10] last summer, a number of new measurements have become available. The MARK II group has installed a new vertex chamber[11] which reduces the mean vertex error in a τ event from 4 mm to 0.9 mm (see Fig. 20). At a beam energy of 14.5 GeV, the beam in the PEP machine has a vertical size σ_V of ~50μ and a horizontal size σ_H ~ 500μ. The mean decay length of a τ at these energies would be about 600μ based on τ, μ universality so that measurement errors are now comparable to the tau flight path.

The lifetime of the τ lepton is a direct test of the universality of the τ couplings to the weak currents. If the τ couplings are the same as those of the muon, then the lifetime is given by

$$\tau_\tau = \frac{m_\mu}{m_\tau}^5 \tau_\mu \, Be = (2.8 \pm 0.2) \times 10^{-13} \text{ sec}$$

where the error comes from the uncertainty in the branching ratio Be for τ to decay to $e\nu\bar{\nu}$ (Be = 17.0 ± 1.1%).

The τ leptons used for this study are produced by the reaction $e^+e^- \to \tau^+\tau^-$.
The flight path in these events is measured from the difference of the known beam position and the reconstructed vertex of three prong decays. The distribution of measured decay lengths is shown in Fig. 21

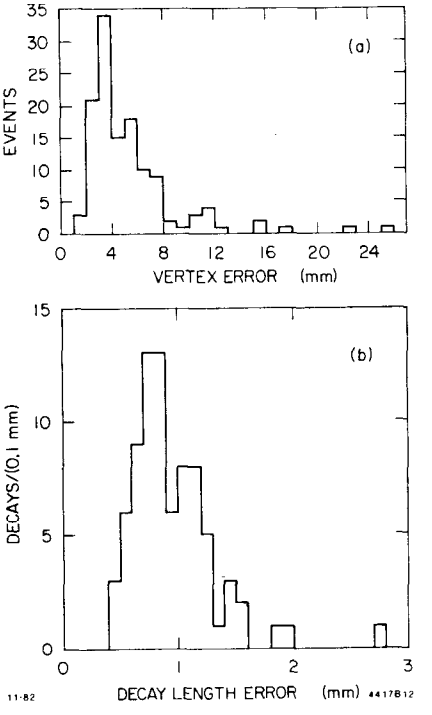

Fig. 20. Vertex error distribution for MARK II τ events for (a) summer 81 data and (b) summer 82 data.

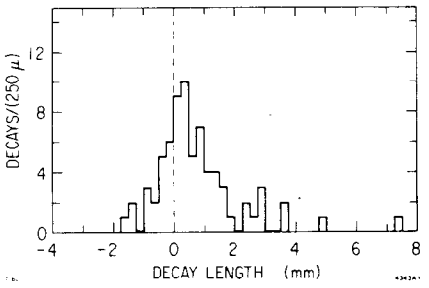

Fig. 21. MARK II distribution of decay lengths for τ events.

and is expected to be the convolution of the resolution with an exponential decay distribution. The fitted decay length for the distribution is

$$\ell = 710 \pm 120\ \mu$$

which must be corrected for a 10% hadronic contamination ($\Delta\ell = 50\mu$) and radiative effects which change the mean center-of-mass energy from 29 GeV to 27.5 GeV. The resulting value for the τ lifetime is

$$\tau_\tau = (3.31 \pm 0.57 \pm 0.60) \times 10^{-13}\ \text{sec} \quad .$$

A similar measurement has been made by the MAC group and the decay path distribution of events and weighted events is shown in Fig. 22. The result of a fit for the τ lifetime is

$$\tau_\tau = (4.1 \pm 1.1 \pm 1.2) \times 10^{-13}\ \text{sec} \quad .$$

Figure 23 shows a compilation of results quoted in the past year from PEP and PETRA detectors on the τ lifetime. The world average from these measurements is 3.5 ± 0.6 which is consistent with the τ-μ universality prediction.

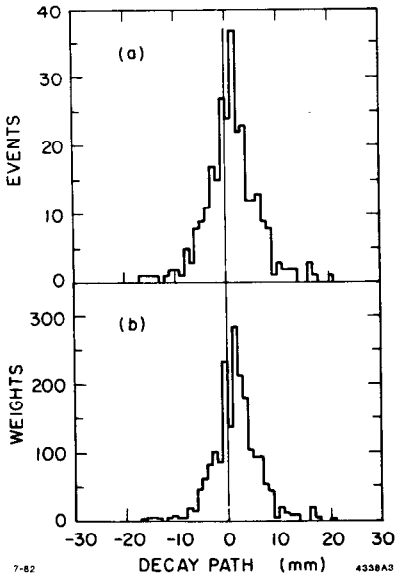

Fig. 22. MAC detector decay path distribution for (a) τ events and (b) weighted τ events.

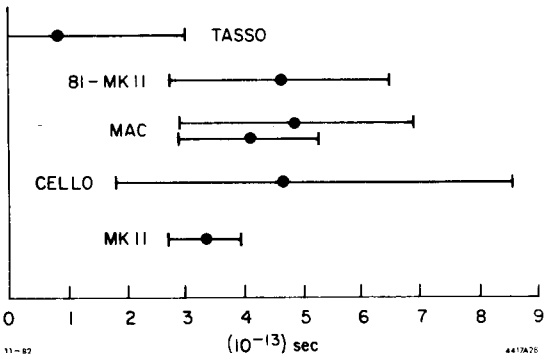

Fig. 23. Compilation of results on the τ lifetime.

VI. INCLUSIVE DISTRIBUTIONS AND SCALING VIOLATIONS

In simple quark parton models at high energies, quark fragmentation functions depend only on the initial quark flavor and the dimensionless ratio x of the fragment's energy to that of the initial quark. This scaling of the fragmentation functions, i.e., dependence only on

$$x = 2E/\sqrt{s}$$

means that the inclusive distribution of particle energies

$$s d\sigma/dx$$

will be independent of center-of-mass energy $\sqrt{s}$.

The MARK II detector using data collected both at the SPEAR storage ring and the PEP storage ring was able to demonstrate a clear violation of this scaling hypothesis.[12] Figure 24 shows that the violations are

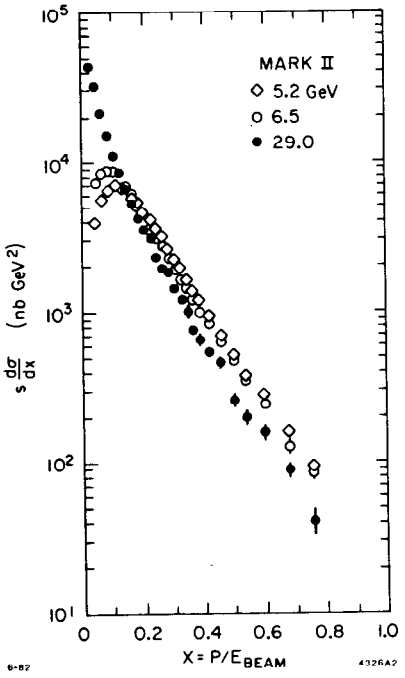

Fig. 24. Comparison of low and high energy inclusive cross sections showing scaling violation.

well outside the 10% relative errors. Several effects can contribute to scale violations. Models with gluon production (QCD) for example have a coupling constant which contains a parameter Λ which sets the scale of the logarithmic variation with Q^2. The scale Λ will thus lead to scale violation. Gluon emission leads to a depletion of the energy available to high x hadrons thus softening the spectrum in qualitative agreement with the behavior seen in Fig. 24. Other effects can also contribute to scale violation. The cross-section at low x for example cannot be expected to scale because of mass effects. These effects for a given mass should persist up to an x value of

$$x \sim 2M/\sqrt{s} \quad .$$

This x value could be as high as 0.25 for example if we use the charm quark mass and $\sqrt{s} \sim 6$ GeV. Thus the scale violation at $x < 0.2$ is probably strictly a mass effect. At high x however, these mass effects should be small and there the observed cross section changes by almost a factor of 2 in going from low to high energies.

The MARK II distributions are in good agreement with the data from the TASSO detector.[13] Figure 25 shows the data from these two detectors as a function of s for each x bin. The QCD expectation is a straight line whose slope determines the Λ parameter. The data have been studied by Peterson et al.[14] who have shown that with a reasonable choice of the charm fragmentation function and using the Altarelli-Parisi evolution equations[15] the data determine a Λ parameter of 200 MeV. They have also shown however that non-perturbative models such as the string model of the

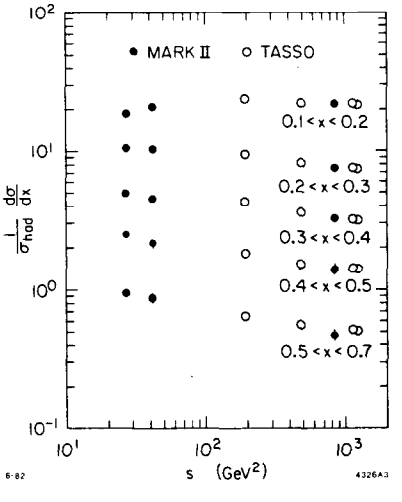

Fig. 25. Inclusive cross section in bins of x for the MARK II and TASSO detectors.

LUND group also fit the data when the charm quark is included. Figure 26 shows the ratio of high and low energy data as determined by the MARK II and TASSO groups compared to perturbative and nonperturbative predictions. This study of the evolution of the structure functions requires information about the charmed and bottom quark fragmentation functions as input and is hence subject to a great deal of uncertainty. It is clear from the curves that the inclusive cross section is quite sensitive to the details of the dynamical model and hence an independent determination of the heavy meson structure functions would allow us to discriminate between these models.

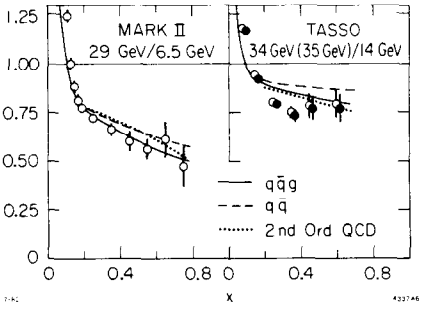

Fig. 26. Ratio of high and low energy data from the MARK II and TASSO groups compared to perturbative and nonperturbative predictions.

VII. CHARM FRAGMENTATION FUNCTION

The MARK II group recently presented a new method of tagging events with charmed mesons in the final state.[16] No evidence for a D meson can be seen in the invariant mass distribution for two particles with assumed π and K masses. However by using the decay sequences

$$D^{*+} \rightarrow D^0\pi^+ \rightarrow K^-\pi^+\pi^+$$

and

$$D^{*-} \rightarrow \bar{D}^0\pi^- \rightarrow K^+\pi^-\pi^- \quad ,$$

the additional kinematic constraint of the mass difference between the D^* and the D allows the identification of a D^* sample.

Figure 27(a) shows the $D^0\pi$, D^0 mass difference for the MARK II data from 31 pb^{-1} at 29 GeV. Clear evidence for the D^* is seen when the momentum fraction of the D^* ($z = 2E_{D^*}/\sqrt{s}$) is above 0.4, while there appears to be little below that value. The data were used to determine the charmed fragmentation function which is found to peak at a value of about 0.5 (see Fig. 27(b)).

The DELCO group has used the same technique to search for a D^* signal. The resolution expected for

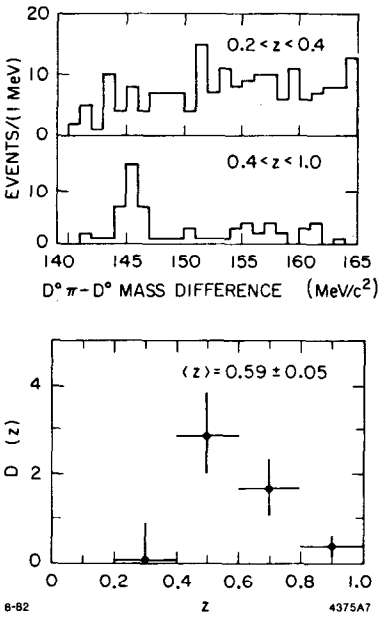

Fig. 27. (a) $D^{o}\pi$-D^{o} mass difference for two values of the D^{*} momentum fraction, and (b) charm fragmentation function determined from the MARK II D^{*} data.

this detector on the $D^{*}D$ mass difference is 2.6 MeV to be compared to 1 MeV for the MARK II. However, the Cerenkov detectors in DELCO can be used to select events where the π and K are identified and this reduces the background in the D^{*} region. The charm fragmentation function based on approximately 20 D^{*} events is shown in Fig. 28.

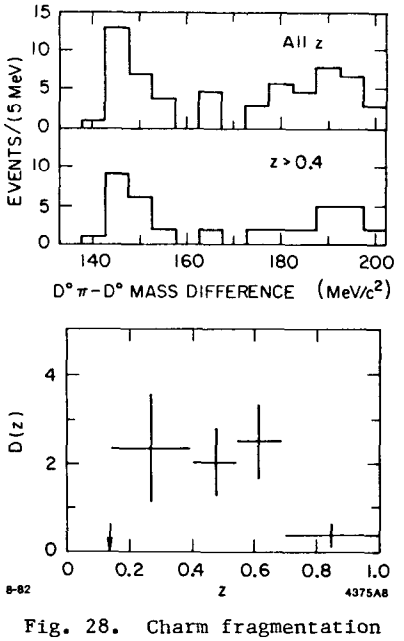

Fig. 28. Charm fragmentation function determined from the DELCO D^{*} data.

The theoretical expectations for heavy quark fragmentation functions have been examined by Brodsky and Peterson[17] who have shown that if the transition

$$Q \rightarrow (Q\bar{q}) + q$$

(where Q is a heavy quark and $(Q\bar{q})$ is a heavy meson) is dominated by kinematics, then the fragmentation function will have the form

$$D_{Q}(z) \sim 1 \Big/ z\left(1 - \frac{1}{z} - \frac{\epsilon_{H}}{1-z}\right)^{2}$$

where

$$\epsilon_{H} = \epsilon_{o}/m_{H}^{2}$$

is a single parameter which determines the shape and m_{H} is the mass of the heavy meson. The parameter ϵ_{o} should be determined by the mass of the light quark and the dynamics of light quark pair production in the fragmentation.

The data from D^{*} production are well represented when the parameter ϵ_{H} equals 0.25. Thus the parameter ϵ_{o} is approximately $(m_{D^{*}}/2)^{2}$. The peaking of the fragmentation function at large values of z, i.e., $\langle z \rangle = 0.5$ means that the momentum spectrum of particles from D and D^{*} decay will contribute at high values of z hence tending to dilute the effect of gluon radiation discussed before which softens the momentum spectrum. K mesons from D decay will also have higher mean momentum values and hence be more difficult to detect using conventional time of flight techniques.

The value of the D^{*} production cross section is also interesting. The measured value from the MARK II group is

$$\sigma(D^{*+} + D^{*-}) = 0.25 \pm 0.13 \text{ nb} \quad .$$

This is to be compared to the point cross sections for charm and bottom quark production at 29 GeV which are

$$\sigma(c + \bar{c}) = 0.27 \text{ nb}$$
$$\sigma(b + \bar{b}) = 0.07 \text{ nb} \quad .$$

The D^{*} production accounts for a major part of the total charm production cross section.

The MARK II group has used the same sample of D^{*} events and the vertex capabilities discussed previously in the τ lifetime section to determine the lifetime of the D^{o} meson. By requiring that the momentum fraction of the D^{*} be greater than 0.6, there remain 7 events with no background. The measured lifetimes of the seven events are shown in Fig. 29. The resulting lifetime for the D^{o} is

$$\tau_{D^{o}} = \left(3.7 \begin{array}{l} +\ 2.5 \\ -\ 1.5 \end{array}\right) \times 10^{-13} \text{ sec} \quad .$$

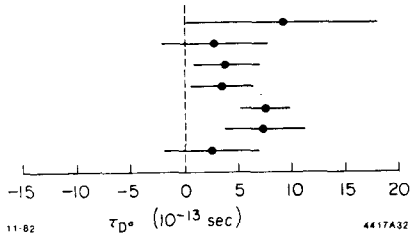

Fig. 29. Measured values of the D^0 lifetimes. MARK II.

VIII. ELECTRONS IN HADRON EVENTS

Scaling violations have shown that an understanding of the effects of heavy mesons is important, and the study of D^* production has indicated that the fragmentation function for heavy quarks is peaked at high z. Both of these studies require an investigation of samples of events which contain heavy c or b quarks as opposed to light u,d,s quarks. The separation of events into classes depending on the type of initial quark is called flavor tagging and it can provide us with significant information about the production of hadronic final states.

It is to be expected that leptons from the decay of heavy objects such as a charmed or bottom meson can have a $p_\perp$ of up to $M_H/2$ where M_H is the meson mass. Since half the meson mass for charmed or bottom mesons is large compared to the mean transverse momentum of particles relative to a hadronic jet, particles with large transverse momenta will tend to be decay products of heavy mesons. A similar argument can be applied to the particles with large fractions of the total longitudinal momentum. If the argument of the preceeding section is correct, then the mean value of z for heavy mesons will be large. This will tend to increase the longitudinal momentum of their decay products.

In a preliminary study of leptons in hadronic events, the MARK II group has used electrons to search for evidence of the semi-leptonic decay of heavy mesons. The usual analysis procedure for locating leptons is to follow a charged track into the liquid argon shower counters and to try to match the position of the track there to the position of reconstructed showers. Since there can be confusion in the core of dense jets in such an approach, the new analysis does not try to use reconstructed showers. Instead, the energy deposited on strips in the liquid argon modules along the direction of the charged track is accumulated for the first eight radiation lengths. Candidate electrons are those with an energy deposit greater than 50% of their momentum. Charged tracks are required to have at least 1 GeV of momentum. This algorithm does not eliminate interacting pions or π^0 overlaps with charged tracks, but its efficiency for electrons is high and roughly independent of confusion due to nearby tracks. In a total sample of 35 pb^{-1}, 10691 hadronic events yield 1013 candidate tracks. Of these, 80 are identified as $e^+e^- \to \gamma\gamma$ or other QED processes, 120 are γ conversions, and 425 are misidentified hadrons. The result is a sample of 388 ± 95 events.

The data are divided into bins of p and $p_\perp$, and the distribution of candidates is fit to the expected distribution assuming as parameters the branching ratios $Br(b \to e)$, $Br(c \to e)$ and the shape parameter ε_b which determines the B meson fragmentation function. The shape of the charm fragmentation function is fixed using $\varepsilon_c = 0.25$ as determined by the D^* studies. The results are

$$Br(c \to e^-) = 0.07 \pm 0.02 \pm 0.02$$
$$Br(b \to e^-) = 0.11 \pm 0.03 \pm 0.02$$
$$\varepsilon_b = 0.04 \,{}^{+\,0.035}_{-\,0.025} \,.$$

The result for the leptonic decay branching ratio for the B meson is in good agreement with recent results from the CUSB ($Br = 0.131 \pm 0.025 \pm 0.03$) and CLEO ($Br = 0.136 \pm 0.021 \pm 0.017$) groups at CESR.[18] For the shape of the bottom fragmentation function, Fig. 30(a) shows the shape represented by the value of $\varepsilon = 0.25$ determined for charm and Fig. 30(b) shows the range of shapes allowed by the fit to the bottom fragmentation function. The trend toward higher mean values of z for the heavier mesons is supported by the data. In fact, the simple argument given in the preceeding section that the parameter ε is related to the mass of the heavy meson by

$$\varepsilon = \varepsilon_o / M_H^2$$

predicts that

$$\frac{\varepsilon_b}{\varepsilon_c} = \frac{m_D^2}{m_B^2}$$

in rough agreement with the measured value 0.04/0.25.

IX. INCLUSIVE MUON FLAVOR TAGGING

The MAC group has also been using inclusive leptons to study flavor tagging. The external muon system is used to identify hadronic events which contain a muon with momentum greater than 2 GeV/c. Events with muons which have large transverse momenta relative to

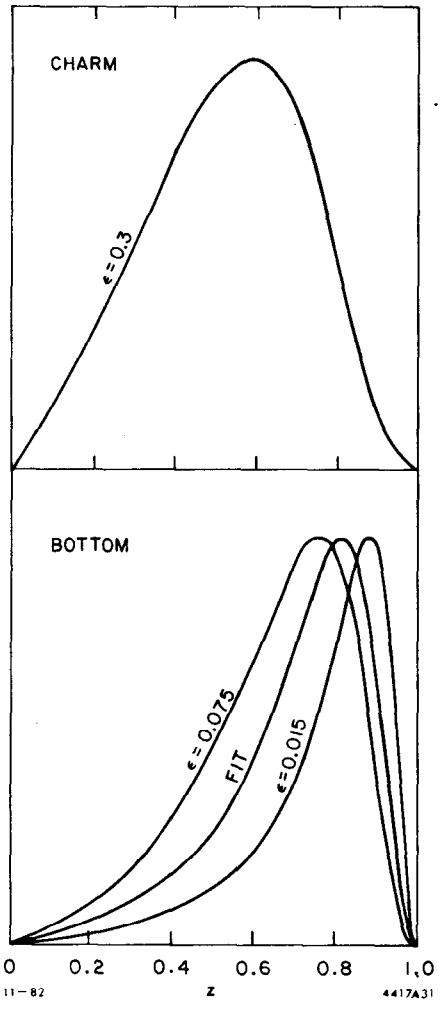

Fig. 30. (a) Charm fragmentation function $\varepsilon = 0.25$; and (b) bottom fragmentation function for the fit value $\varepsilon = 0.04$ and one sigma errors.

the jet axis should come from the decay of heavy mesons. The mass of the jet opposite the detected muon is defined as

$$M_J = E_b(1 - T_{\frac{1}{2}}^2)^{\frac{1}{2}}$$

where E_b is the beam energy and $T_{\frac{1}{2}}$ is the thrust of the jet. Figure 31(a) and (b) show the the distribution of jet mass for events with muon $p_\perp$ less than and greater than 1 GeV respectively. The contribution from B decays is enhanced by a factor of four in the second sample. The curve is a Monte Carlo calculation which uses the leptonic branching ratio for B mesons measured by the CLEO group. By using the separation of the vertices of the two jets in the b enhanced sample, the MAC group has determined a 95% confidence level upper limit for the B lifetime of

$$\tau_b < 3.7 \times 10^{-12} \text{ sec} .$$

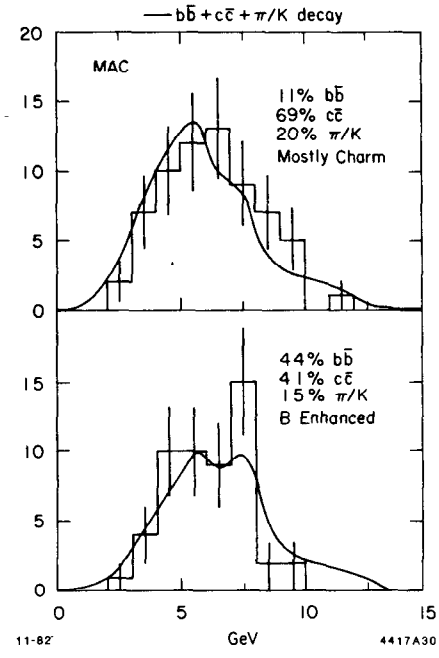

Fig. 31. MAC jet mass distribution for muon transverse momentum (a) less than and (b) greater than 1 GeV/c.

X. ENERGY-ENERGY CORRELATIONS

Tests of QCD have often relied heavily on Monte Carlo calculations to parameterize the fragmentation of quarks, effects of heavy meson decays, perturbative gluon emission, gluon fragmentation, and even non-perturbative effects. While some of the parameters of the models can be fixed by comparison with low energy data, uncertainties must arise for example in the parameterization of gluon fragmentation which is not observed at low energies. Assumptions must be made about the energy dependence of each of the parameters, and then comparisons can be made at high energy to extract for example the probability of perturbative gluon emission from three jet event rates. Often, however uncertainties in fragmentation phenomena make it difficult to separate the genuine properties of QCD from the details of the Monte Carlo model.

To test QCD in a clean way, it is desirable to find quantities which are as insensitive as possible to details of the fragmentation process and yet are still calculable within the framework of the theory. To avoid singularities in QCD, it is important to choose observables which are insensitive to the production of soft gluons or gluons which are collinear or anticollinear with a quark. These types of observables should also be less sensitive to fragmentation effects.

Several authors[19] have suggested measurements which have the desired properties. The energy weighted

angular distribution or "antenna" pattern eliminates the soft gluon singularity because of the energy weighting. Also, when the energy is collected in finite elements of solid angle, it is included regardless of whether it originated from a gluon or a quark and in this case, collinear gluon emission has no effect. The main features of this cross section are two lobes of energy due to the primary quark antiquark pair. The minima between the lobes are sensitive to gluon radiation and could be used to determine its probability and hence the strong coupling constant. However, these minima are also filled in by quark fragmentation, the only difference being a $\ell n\sqrt{s}$ behavior for the gluon effect and a $1/\sqrt{s}$ dependence for fragmentation effects. Thresholds due to heavy meson production will also change the energy observed near the minima and untangling all of these effects is difficult. A second measurement, the energy-energy correlation, requires the measurement of correlations between two energy deposits into solid angles $d\Omega$ and $d\Omega'$. The two elements of solid angle are specified by four angles $(\theta,\phi,\theta',\phi')$. Usually the cross section is integrated over the angles leaving fixed the relative angle χ between $d\Omega$ and $d\Omega'$. This cross section can be evaluated in QCD and neglecting fragmentation effects has the form

$$\frac{1}{\sigma}\frac{d^2\Sigma}{d\Omega d\Omega'} = \mathscr{A}^{QCD}(\chi)\ \frac{1}{\sigma}\left(\frac{d\sigma}{d\Omega}+\frac{d\sigma}{d\Omega'}\right)$$

$$+\ \mathscr{B}(\chi)\ \frac{3}{16\pi}\ (\cos\chi+\cos\theta\cos\theta')\ .$$

The functions $\mathscr{A}$ and $\mathscr{B}$ are known and are proportional to the strong coupling constant α_s. The most interesting feature of this measurement was originally thought to be the asymmetry

$$\mathscr{D}(\chi) = \frac{d\Sigma}{d\cos\chi}(\pi-\chi) - \frac{d\Sigma}{d\cos\chi}(\chi)$$

since for a $q\bar{q}$ initial state, fragmentation contributions do not change $\mathscr{D}(\chi)$. Since $\mathscr{A}$ and $\mathscr{B}$ contain asymmetric pieces proportional to α_s it was thought that this would provide a fragmentation independent measure of α_s. The reason this is not true was pointed out recently by the MARK II collaboration[20] and is illustrated in Fig. 32. While the $q\bar{q}$ topology has symmetric fragmentation contributions, the $q\bar{q}g$ initial state has both an asymmetry in the energy-energy correlations of the partons and an asymmetric fragmentation contribution. Both of these terms will be proportional to α_s. The nonperturbative contributions must be estimated by Monte Carlo and limit the precision with which the strong coupling constant can be determined.

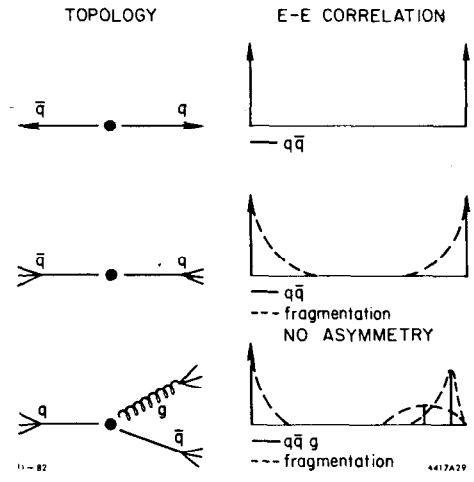

Fig. 32. Topology and contributions to energy-energy correlations for $q\bar{q}$ and $q\bar{q}g$ partons. The solid lines are the parton contributions and the dashed lines indicate the effects of fragmentation.

The data taken by the MARK II collaboration are shown in Fig. 33. In determining the value of α_s the three parton fragmentation contribution was assumed to be of the form

$$\alpha_s \frac{A_1}{\sqrt{s}\ \sin^3\chi} \quad \text{for} \quad \chi < 90^o$$

and $\alpha_s A_1(1+\cos\chi)/\sqrt{s}$ for $\chi > 90^o$ which agrees well with the Monte Carlo simulation. The coefficient A_1 is a free parameter of the fit. An additional term

$$A_0/\sqrt{s}\ \sin^3\chi$$

is used to parameterize fragmentation contributions from $q\bar{q}$ events. The result of the fit is

$$\alpha_s = 0.19 \pm 0.02 \pm 0.03$$

$$A_0 = (0.7 \pm 0.2)\ \text{GeV}$$

$$A_1 = (2.6 \pm 0.5)\ \text{GeV}\ .$$

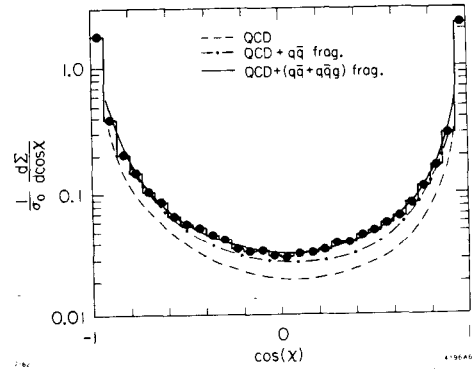

Fig. 33. MARK II energy-energy correlations as a function of $\cos\chi$. The solid curve is the QCD prediction plus nonperturbative contributions.

Fragmentation terms account for ≈40% of the observed cross section near $\chi = 90^o$ (see Fig. 33).

A similar analysis has been carried out by the MAC collaboration. The detector is able to use 97% of 4π calorimetry to determine the energy flow. The data are shown in Fig. 34, with curves corresponding to the results of the fit which are

$$\alpha_s = 0.16 \pm 0.006 \pm 0.02$$
$$A_0 = 1.2 \pm 0.08 \pm 0.15 \text{ GeV}$$
$$A_1 = 2.5 \pm 0.2 \pm 0.4 \text{ GeV} .$$

The agreement between the experiments using this technique to measure α_s is good as is the agreement with previous measurements near 30 GeV using for example the fraction of observed three jet events. What we have learned in the past year however is that the fragmentation corrections to the asymmetric part of the energy flow are important and are the major contributors to the systematic errors on α_s. Without these contributions, the asymmetry would have measured α_s directly. Since the asymmetry is not a fragmentation free measure of α_s, it is more relevant to look at the double energy cross section directly. As can be seen from Figs. 33 and 34, QCD together with the $q\bar{q}g$ fragmentation contribution fit the data quite well. While the fragmentation sensitivity is somewhat disappointing, it does not lead to larger systematic errors in α_s than those of previous measurements.

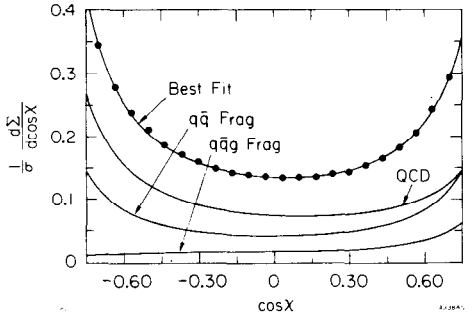

Fig. 34. MAC energy-energy correlations showing the QCD, $q\bar{q}$ fragmentation and $q\bar{q}g$ fragmentation contributions.

XI. TOTAL HADRONIC CROSS SECTION

While the previous measurement has mainly theoretical problems barring its use as a measure of the strong coupling constant, the total cross section has mainly experimental uncertainties. Many authors have pointed out that a high accuracy measurement of the total cross section is a clean test of QCD. The ratio of the hadronic cross section to the point cross section is

$$R = \frac{\sigma_{had}}{\sigma_{point}} = \frac{4\pi}{3}\frac{\alpha^2}{s}\left[\sum e^2_{quarks} \cdot 3 + \frac{1}{4}\sum e^2_{scalars}\right]$$
$$\left(1 + \frac{\alpha_s}{\pi} + C_2\left(\frac{\alpha_s}{\pi}\right)^2 + \ldots\right) .$$

The coefficient C_2 is known to be small, and neglecting the possibility of fundamental scalars, at 29 GeV we would have

$$R_{QCD} = 3.67\left(1 + \frac{\alpha_s}{\pi} + \ldots\right) \approx 3.9 ,$$

so that we need to detect a ΔR of ~0.2. While most experiments currently have statistical errors of approximately 0.05, the systematic errors are between 0.25 and 0.14.

The MAC group has used their full solid angle (~97% of 4π) to measure R and have found

$$R = 3.93 \pm 0.04 \pm 0.12 \pm 0.12$$

where the errors are statistical, systematic, and systematic due to unknown higher than α^3 radiative corrections. Most previous measurements of R have used smaller acceptances and hence have increased systematic errors due to larger acceptance corrections. However they have smaller errors in the contributions from uncertainties in the edges of the acceptance and from radiative corrections. The MAC group has used the same data restricting the sample to those events where the thrust axis lies in the polar angle range of 55^o-125^o to determine

$$R = 3.87 \pm 0.05 \pm 0.10 \pm 0.10 .$$

The MARK II group has also measured this cross section and finds

$$R = 3.90 \pm 0.05 \pm 0.25 .$$

Lower energy measurements using the same apparatus gave

$$R = 3.90 \pm 0.02 \pm 0.25 \text{ at } 5.2 \text{ GeV}$$

and

$$R = 3.95 \pm 0.05 \pm 0.25 \text{ at } 6.5 \text{ GeV} .$$

The relative systematics between the low and high energy data are 5%.

Unfortunately it is difficult to reduce the systematic errors since they are the sum of many different contributions; two photon events, τ pair production, radiative correction uncertainties, effects of analysis cuts on multiplicity and event topologies, backgrounds, fiducial cuts, quark mass effects, residual charm and bottom threshold effects, weak corrections, etc. It is difficult to see how the sum of all of effects could be made small compared to the total QCD effect of only 5%. This problem is not solved by going to higher

energies since at higher energies (~50 GeV) the effects of QCD and weak neutral current corrections can be comparable!

XII. SUMMARY

A brief review has been given of the physics which has been done at PEP with particular emphasis on data obtained in the past year. Tests of QED show no evidence for nonpointlike behavior of the leptons or for contributions from massive leptons. Tests of the weak couplings of the leptons are in agreement with the standard unified weak and electromagnetic model. The five prong branching ratio of the τ lepton has been shown to be small and cannot account for missing τ decay modes. Tests of τ universality have been improved both by high accuracy measurements of τ pair production and increasingly accurate measurements of the τ lifetime. Scale violation effects have been found to be consistent with a Λ parameter of 200 MeV although it has become clear that the details of nonperturbative effects and charm fragmentation are important in this analysis. The charm fragmentation function has been measured using the production of D^*'s and first attempts to measure the bottom fragmentation function indicate that it like charm is peaked at high z. Searches for tests of QCD which are less dependent on fragmentation models than three jet measures have found that energy-energy correlations are also affected by fragmentation corrections. While the asymmetry in the energy correlations cannot be used to measure α_s directly, a fit to the shape of the correlations yields a value of α_s in agreement with other measurements. The total hadronic cross section has also been measured. It would provide a good test of QCD, but at present, systematic errors are comparable to the expected effect.

REFERENCES

1. K. Kinoshita, P. Price, D. Fryberger, Phys. Rev. Lett. 48, 77-80 (1982).
2. M. Capdequi-Peyraneyre et al., Nuovo Cimento 63A, 501 (1981).
3. N. M. Kroll, Nuovo Cimento 45, 65 (1966); J. A. McClure and S. D. Drell, Nuovo Cimento 37, 1638 (1965).
4. F. A. Berends and R. Kleiss, Nucl. Phys. B186, 22 (1981).
5. P. Dittmann and V. Hepp, Z. Phys. C10, 283 (1981).
6. R. Budny, Phys. Lett. 55B, 227 (1975).
7. See for example, J. Kim, P. Langacker, M. Levine, and H. Williams, Rev. Mod. Phys. 53, 211 (1981).
8. T. Himel et al., Phys. Rev. Lett. 41, 449 (1982).
9. C. Blocker et al., SLAC-PUB-2948 (1982), submitted to Phys. Rev. Lett.
10. G. Feldman et al., Phys. Rev. Lett. 48, 66 (1982).
11. J. Jaros, SLAC-PUB-2992 (1982).
12. J. Patrick et al., SLAC-PUB-2936 (1982).
13. R. Hollebeek, 1981 International Symposium on Lepton and Photon Interactions at High Energies, Bonn, Germany, August 24-29, 1981, p. 1.
14. C. Peterson, D. Schlatter, I. Schmitt and P. Zerwas, SLAC-PUB-2912 (1982).
15. G. Altarelli and O. Parisi, Nucl. Phys. B126, 298 (1977).
16. J. Yelton et al., SLAC-PUB-2926 (1982).
17. S. Brodsky and C. Peterson, Phys. Rev. D23, 2745 (1981).
18. K. Chadwick et al. (CLEO Collaboration), CLNS 82/546.
19. G. Sterman and S. Weinberg, Phys. Rev. Lett. 39, 1436 (1977); G. Fox and S. Wolfram, Nucl. Phys. B149, 413 (1979); C. Basham, L. Brown, S. Ellis and S. Love, Phys. Rev. D17, 2298 (1978).
20. D. Schlatter et al., Phys. Rev. Lett. 46, 1659 (1981).